Surface modification of $Cu(In,Ga)Se_2$ thin films by radio frequency magnetron sputtering with a gradient power

NINGYU REN, JUN ZHU*, YANLAI WANG, SHILIANG BAN*

School of Physical Science and Technology, Inner Mongolia University, Key Laboratory of Semiconductor Photovoltaic Technology at Universities of Inner Mongolia Autonomous Region, Hohhot 010021, PR China

Copper indium gallium selenide ($Cu(In,Ga)Se_2$, CIGS) thin films were fabricated using radio frequency magnetron sputtering from a single quaternary ceramic target followed by the rapid thermal annealing treatment. The target was made of Cu_2Se, Ga_2Se_3, and In_2Se_3 powder and Cu:In:Ga:Se=20:17.5:7.5:55 at%. By adopting a gradient sputtering power, i.e., a constant 45 W for the first 120 min and a step power from 45 to 50 W for the last 30 min, the films had a Cu-poor smooth surface and showed favorable chemical stoichiometry. After selenization, Cu/(In+Ga) ratio was examined as about 0.80-0.95 and Ga/(In+Ga) ratio about 0.20-0.30.

(Received February 23, 2017; accepted February 12, 2018)

Keywords: CIGS, Film, Quaternary target, RF magnetron sputtering, Tunable power

1. Introduction

$Cu(In,Ga)Se_2$ (CIGS) has been a promising chalcopyrite absorber material for high-efficiency polycrystalline thin film solar cells because of its tunable band-gap (1.02-1.67eV) and the highest absorption coefficients ($\alpha>10^5 cm^{-1}$) [1-2]. Due to the development of experimental techniques, the conversion efficiency of CIGS solar cells has been continually increased. The latest report shows that the efficiency of CIGS solar cells has reached up to 22.6% [3]. Several methods, mainly including co-evaporation from pure elemental sources and selenization of elemental or compound precursor layers, have been employed to fabricate CIGS absorber films [2, 3, 4-7]. However, multiple-source co-evaporation has its drawbacks in industry-scale solar cell production because of the challenge for equipment and the difficulty in controlling the uniformity of the films on large area [4]. On the contrary, deposition of metallic precursors with Cu, In and Ga elements which are subsequently selenized by H_2Se [8] or Se [9, 10] vapor is a stable and reproducible technique for mass production with the capability for large-area deposition [11]. Moreover, the film deposited by magnetron sputtering technology has strong adhesion with substrate and is very uniform in morphology and element distribution. In recent years, some groups have tried to deposit CIGS thin films by magnetron sputtering using a single quaternary target with or without post-selenization, but the properties of films still need to be improved [2, 12-19]. The main obstacle is that the different deposition rates on the Mo substrate for different elements cause a large stoichiometric deviation between the standard target material and the sputtered CIGS absorber layer. Besides, the poor crystallinity of the as-deposited CIGS layer from the direct single target sputtering also gives rise to the performance degeneration of CIGS cells. During selenization treatment, another problem is that large particles are easily formed at the Cu-rich surface (SR-Cu) which worsens the cell performance while the Cu-poor surface (SP-Cu) of an absorber layer will improve the device efficiency. As known, $Cu_{2-x}Se$ is the main factor of larger-particle precipitation. There are several ways to restrain this phenomenon. Among them, wet chemical treatment using highly toxic KCN or other solutions has not a very beneficial effect on $Cu_{2-x}Se$ phase [20].

In this paper, we have developed an experimental method to reduce larger-particle precipitation and hence to improve the structural homogeneity of CIGS films. Firstly, a customized copper-poor and selenium-rich quaternary target instead of the standard stoichiometric one was used to deposit precursor films. The target was made of Cu_2Se, Ga_2Se_3, and In_2Se_3 powder and Cu:In:Ga:Se=20:17.5:7.5:55 at%. During this process, element Cu near the surface was further reduced by adjusting the radio frequency (RF) power. A simplified selenization technology was employed to supplement Se. What is more, the commonly used H_2Se, which is expensive, highly toxic and explosive, was replaced by solid Se powder as Se source. The structural, morphology and element composition were analyzed by X-ray diffraction (XRD), Raman spectroscopy, scanning electron microscope (SEM), energy-dispersive spectrometer (EDS) and X-ray photoelectron spectrometer (XPS).

2. Experimental

Soda-lime glass covered with a Mo back-contact was used as substrate. The CIGS precursor thin films were subsequently grown by RF sputtering using a customized quaternary $Cu_{0.8}In_{0.7}Ga_{0.3}Se_{2.2}$ target. Prior to the deposition, the chamber was first evacuated to a base pressure of 5×10^{-4} Pa by a turbo molecular pump. Then, the pre-sputtering was conducted under the condition of an elevated RF power about 20 W for 5 min to clean the target surface. The substrate-to-target distance was 70 mm and the working pressure was 0.5 Pa. The circulating cooling water system was applied for the whole deposition process which kept the sputtering system at 15 °C. The sputtering conditions are summarized in Table 1. During the sputtering process of depositing films, RF power was tunable with a fixed Ar flow of 30 sccm.

Table 1 Process parameters for depositing CIGS precursor films

Deposition parameter	*Sputtering condition*
Target	*99.99 wt.% CIGS*
The diameter of target	*50 mm*
Target-to-substrate distance	*70 mm*
Substrate	*Soda-lime glass covered with a Mo back-contact*
Substrate temperature	*Room temperature*
Base pressure	*5×10^{-4} Pa*
Sputtering medium	*Ar (purity 99.99%)*
Gas flow	*30 sccm*
Working pressure	*0.5 Pa*

It is found that Cu-poor surface of absorber layer is beneficial for the cell device. In order to realize the Cu-poor surface, a gradient sputtering power was adopted during CIGS precursor film growth. As depicted in Fig. 1, a constant power of 45 W was used to sputter for 120 minutes in the first stage. In the second stage, a step sputtering power from 45 to 50 W was used for 30 minutes. For comparison, SR-Cu samples were grown by sputtering 150 min with a constant power of 45 W.

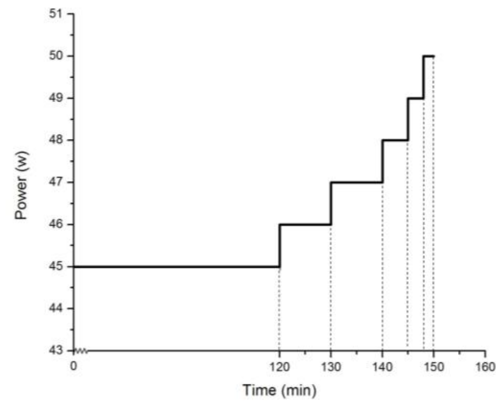

Fig. 1. Adjusting sputtering power of SP-Cu samples as a function of time.

For the annealing treatment, a rapid thermal process (RTP) was performed in a simple furnace, equipped with a quartz tube as a reaction chamber. The annealing system is depicted in Fig. 2. Both the as-deposited CIGS precursor film and 100 mg Se powder in a graphite box were put into the reaction chamber and Ar was used as the carrier gas. Se source was located about 100mm away from the precursor which was inverted in the graphite box. Ar flew through the tube and was discharged into the beaker filled with water during the whole annealing process. The sample was heated to 550 °C for 200 s and kept at this temperature for 30 min. Finally, the sample was cooled down naturally.

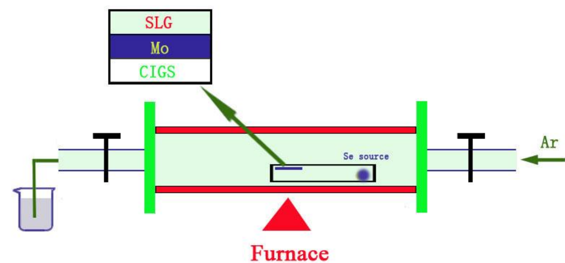

Fig. 2. Schematic diagram of the selenization furnace

Crystallographic structures and phases of the CIGS thin films were examined by XRD analysis (D8-ADVANACE). A SEM (S-3400) coupled with an EDS was utilized to detect the morphology and composition of the film surface and cross-section of the samples.

3. Results and discussion

To study the influence of sputtering power on the composition of precursor films, we used the quaternary $Cu_{0.8}In_{0.7}Ga_{0.3}Se_{2.2}$ target to make samples on glass substrate with RF power changing from 40 to 80 W. It is known that stoichiometric ratios of Cu/(In+Ga) and Ga/(In+Ga) of CIGS thin films are the key parameters to characterize the performance of films. The atomic ratios of Cu/(Ga+In), Ga/(Ga+In) and Se/(Cu+In+Ga) of the samples are shown in Fig. 3 (a) and the content of each element in Fig. 3 (b). As can be seen, the concentration of Cu and the ratio of Cu/(In+Ga) prominently decreased with the increase of power. Cu/(In+Ga) ratio ranges from 0.5 to 1.1 and Ga/(In+Ga) ratio from 0.20 to 0.30. The films changed from the Cu-rich state to the Cu-poor state when increasing sputtering power beyond 50 W. The content of element Se in all films is excessive, which is usually expected for CIGS absorber films.

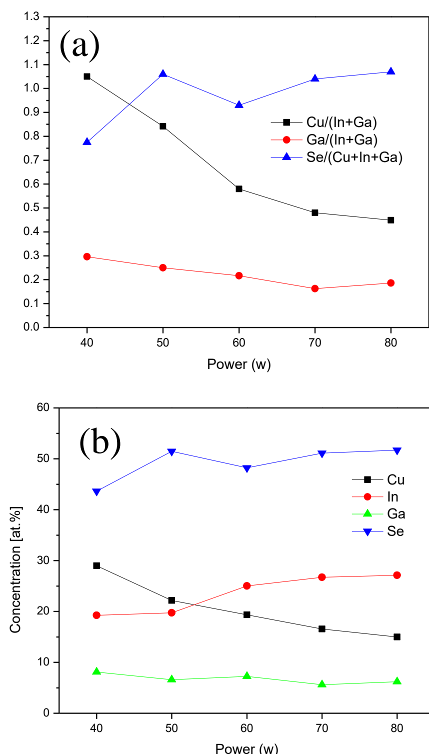

Fig. 3. Atomic ratios of Cu/(Ga+In), Se/(Cu+In+Ga) and Ga/(Ga+In) (a) and chemical composition (b) of the precursor films on glass substrates.

According to the above analysis, we further fabricated the SP-Cu samples using the tunable power shown in Fig. 1 and the SR-Cu samples using a fixed power of 45 W on soda-lime glass with Mo back-contact.

Fig. 4 gives the SEM micrographs of the two kinds of samples selenizating at 550 °C. In Fig. 4 (c), large particles, also called as “polygon grains”, were observed on the surface of SR-Cu samples, leading to a rough top surface. It is found that the abundant Cu_2Se and $CuInSe_2$ phases cause the larger-particle precipitation [10, 21]. As shown in Fig. 4 (d), if adopting the tunable power, compacter and smoother SP-Cu samples were obtained and less irregular grains appeared at the surface. The surface morphology of the film was mainly a mixture of grains in the size of 200 to 2000 nm. The SP-Cu film was significantly improved and the grains showed an obvious sphalerite structure. It should be pointed out that although the SP-Cu samples demonstrate almost uniform grain throughout the film, some cracks and voids can be obviously seen near the Mo back contact in Fig. 4 (b). The occurrence of this bilayer structure could be attributed to other secondary phases such as Cu_2Se and InSe [10, 22]. Raman spectroscopy is a powerful tool for the analysis of CIGS films and Raman spectra may contain valuable information concerning secondary phases. Comparing Fig. 4 (e) to (f), displays the Raman pattern of SP-Cu and SR-Cu samples of CIGS. The intense peak of 174 cm-1 observed in SP-Cu and SR-Cu samples. It is known that this peak is the A1 mode of CIGS films. Mixed B2/E modes are also observed at around 213 cm-1 from all the CIGS films. From Fig. 4(e) and (f), it is observed that a distinct peak around 260 cm-1 is found for SR-Cu sample, peaks at around 258-260 cm−1 related to Cu2-xSe phase disappeared for SP-Cu sample, which can confirm Cu2-xSe phase prefers to segregate at film surface. Raman spectrum measured at point A inside the particle indicates this result. Some pesks at 210, 230, 260 cm^{-1} are relating to In_aSe_b and $Cu_{2-x}Se$ [21].

Table 2. The at% measured by EDS analysis for as-deposited CIGS absorption thin film converted from precursors after selenization process.

at%	Cu	In	Ga	Se	CIG	GGI	Se/metal
Target	20.00	17.50	7.50	55.00	0.80	0.30	1.22
Compositions of precursors and selenized SP-Cu samples							
Precursor	22.03	21.91	6.88	49.19	0.76	0.24	0.97
Selenized	22.21	20.02	5.04	52.74	0.92	0.20	1.11
Compositions of precursors and selenized SR-Cu samples							
Precursor	23.23	19.05	5.62	52.11	0.94	0.23	1.09
Selenized	21.80	16.51	4.99	56.70	1.01	0.23	1.31

**CIG: Cu/(In+Ga), GGI: Ga/(In+Ga), Se/metal: Se/(Cu+In+Ga).*

The element compositions of the CIGS absorber thin films were identified by EDS. The data of SP-Cu and SR-Cu samples are listed in Table 2 for comparison. After selenization, the films exhibited favorable stoichiometric ratio with Cu/(In+Ga) being about 0.80-0.95 and Ga/(In+Ga) about 0.20-0.30. Our results are well matched with Ref. [18]. It can be also seen that Cu is exactly reduced by adjusting sputtering power. This also leads to a flatter film as shown in Fig. 4 (f).

Se was compensated during the selenization process.

But the content of Ga was slightly lost in the selenization. It could be considered that the Ga atoms are diffused toward the interface between Mo film and CIGS absorber layer [10]. Also, elemental mapping of the SP-Cu sample was shown in Fig. 5. It reveals that elements Cu, In, Ga and Se are evenly distributed in the absorber layer after annealing which indicates that CIGS polycrystalline thin films were obtained by adopting the tunable power.

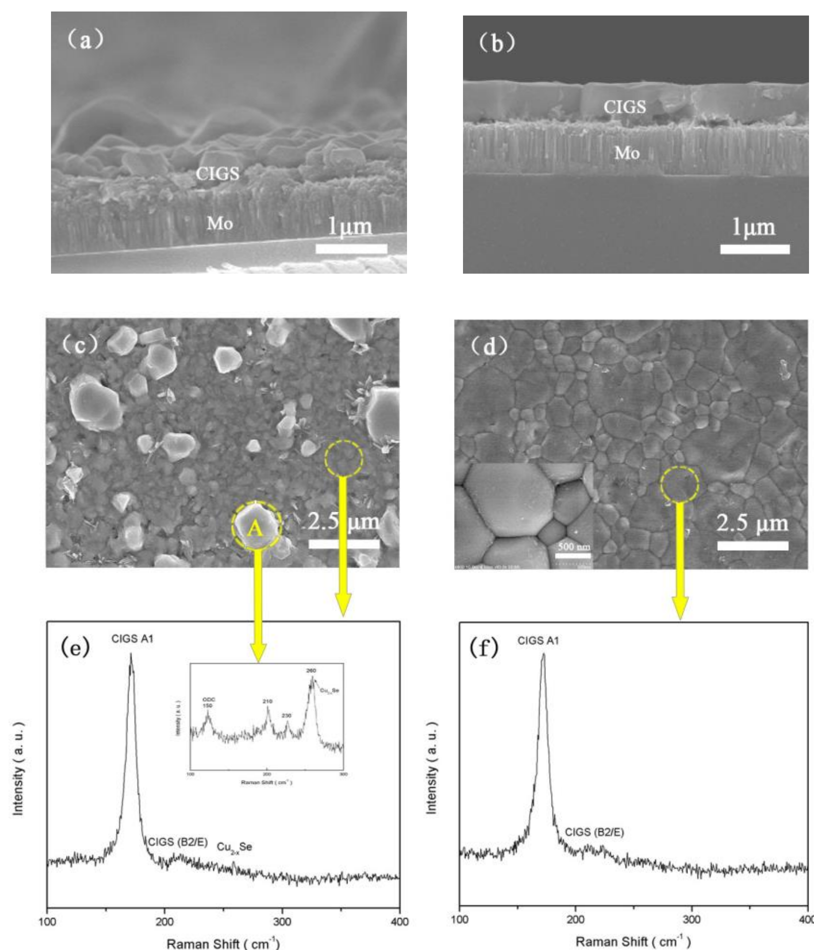

Fig. 4. SEM topography and cross-section images of SP-Cu samples (b), (d) and SR-Cu samples (a), (c), Raman spectrum of SP-Cu samples (f) and SR-Cu samples (e) after heating at 550 °C.

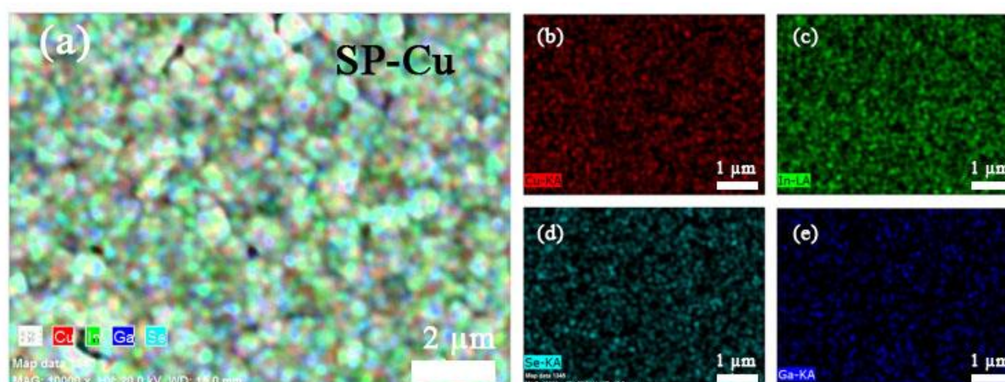

Fig. 5. High resolution elemental mapping and the corresponding individual elemental mapping of Cu, In, Ga and Se for SP-Cu samples after heating at 550 °C.

In order to compare Cu content at the surface of SP-Cu and SR-Cu samples, the XPS depth profile measurement was carried out with a depth about 500Å from the surface of films. Fig. 6 shows the XPS intensity of Cu of two types of samples. The Cu2p spectra for samples are shown in Fig. 6. The $Cu2p_{3/2}$ peak intensity of Cu in the SP-Cu surface was higher than that in SR-Cu sample. A lower Cu content was detected on the surface

of SP-Cu sample and the binding energy of Cu decreases with an increase of Cu ratios from SR-Cu to SP-Cu samples. Our result agrees with that in Ref. [23, 24]. It is possible that this is because $Cu_{2-x}Se$ phase appears in SR-Cu sample. Sheu et al. [24] pointed out that the Cu/(In+Ga) ratios are controlled at the range from 0.7 to 0.95 to avoid the formation of $Cu_{2-x}Se$ phase and the binding energy of Cu decreases while Cu/(In+Ga)>0.95. SR-Cu sample with Cu/(In+Ga)=1.01 distinctively revealed a secondary $Cu_{2-x}Se$ phase at around 260 cm^{-1} whereas the SP-Cu sample showed no indication of the secondary phase in Raman spectra. At the same time, a lot of large and deep holes are easily observed in top-view SEM sample Fig. 4(c). It is also may be attributed to the release of Cu from its equilibrium lattice position by the formation of a V_{Cu} and Cu migration into the bulk [25]. The XRD spectra of CIGS absorber films are shown in Fig. 7. The peaks at 2θ = 40.5° are attributed to Mo (110) and the other peaks can be attributed to CIGS. The strongest characteristic peak of all films is (112) peak. The diffraction peaks of SP-Cu samples at 2θ = 26.75°, 44.399° and 52.639° correspond to CIGS (112), (204/220) and (312/116) directions (JCPDS Number 35-1102), respectively. They are all consistent with a standard tetragonal (chalcopyrite) structure. The (112) peak is sharp and no extra satellite peaks are found to indicate the good crystallinity and phase purity of the selenized CIGS films. Compared with SR-Cu sample, our experimental results present the positions of (112) and (220/204) diffraction peaks for the SP-Cu sample demonstrate a shift to lower diffraction angle are also inserted in Fig. 7, which revealed a increase in the lattice parameters. Christopher et al. [26] pointed out that lattice parameter variation due to Cu/(Ga+In) and SP-Cu sample has a bigger lattice parameter than SR-Cu sample. Similar results were found in ref. [27-29]. What is more, it is observed that SP-Cu sample exhibits an obvious (112) preferred orientation and the intensity of SP-Cu sample is higher than SR-Cu sample. The FWHM (full width at half maximum) of (112) peaks are calculated as 0.168 and 0.189 for SP-Cu and SR-Cu samples. The reasons are as follows. The polar (112) surface of CIGS is considerably more stable than the nonpolar (220/204) surface for Cu-poor CIGS thin films, where its surface reconstructs through the formation of In-on-Cu antisite (In_{Cu}) and Cu vacancies(V_{cu}) defects to lower the dipole energy [24, 30, 31]. Therefore, it is reasonable that SP-Cu sample can promote the (112) surface growth. However, no peak related to impurity phases, e.g., Cu_2Se and $CuInSe_2$, could be determined from the XRD pattern of films.

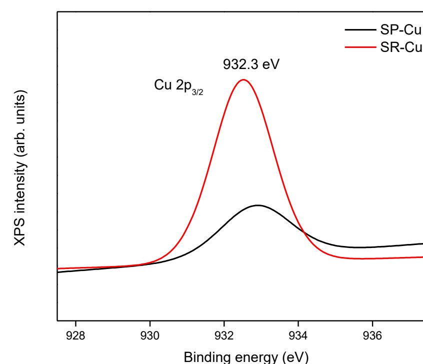

Fig. 6. XPS intensity of Cu of SP-Cu and SR-Cu samples after heating at 550 °C.

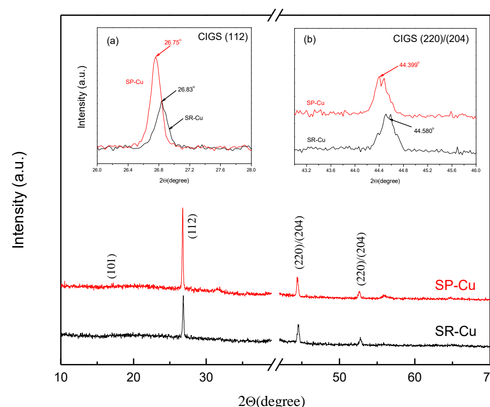

Fig. 7. XRD patterns of SP-Cu and SR-Cu samples after heating at 550 °C. Insets: (a) enlarged XRD peaks of SP-Cu and SR-Cu samples from 26° to 28° and (b) enlarged XRD peaks of SP-Cu and SR-Cu samples from 43° to 46°.

4. Conclusions

In conclusion, CIGS absorber films were fabricated by two-step method. SP-Cu precursor films were deposited by RF magnetron sputtering with a tunable power from a single quaternary Cu0.8In0.7Ga0.3Se2.2 target. The high quality CIGS absorber films with compact grains and smooth surface were obtained after the RTP annealing treatment using Se powder as Se source. The phase structure, elemental composition and surface morphology of as-grown films were analyzed based on XRD, XPS, SEM and EDS measurement. With an adjustment of sputtering power, all the absorber films showed favorable stoichiometric ratio with Cu/(In+Ga) ratio about 0.80-0.95 and Ga/(In+Ga) ratio about 0.20-0.30 for high performance CIGS solar cells. The deposited films showed polycrystalline chalcopyrite structural CIGS phase with a preferential orientation along the (112) direction. Less impurity phases were found at the surface. It is believed that our approach could provide desirable compositional and structural

properties of CIGS absorber films and will possibly reduce the complexity in production process and costs.

Acknowledgments

This work was supported by the National Natural Science Foundation of China (No.61464009, No.51364025) and the Major Fundamental Research Program of Inner Mongolia Autonomous Region (No. 20130902).

References

[1] A. Polman, M. Knight, E. C. Garnett, B. Ehrler, W. C. Sinke, Science **352**, aad4424 (2016).
[2] J. A. Frantz, J. D. Myers, R. Y. Bekele, V. Q. Nguyen, B. M. Sadowski, S. I. Maximenko, M. P. Lumb, R. J. Walters, J. S. Sanghera, IEEE J. Photovolt. **6**(4), 1036 (2016).
[3] P. Jackson, R. Wuerz, D. Hariskos, E. Lotter, W. Witte, M. Powalla, Phys. Status Solidi RRL **10**, 583 (2016).
[4] M. Kemell , M. Ritala, M. Leskelä, Crit. Rev. Solid State Mater. Sci. **30**(1), 1 (2005).
[5] S. Niki, M. Contreras, I. Repins, M. Powalla, K. Kushiya, S. Ishizuka, K. Matsubara, Prog. Photovolt: Res. Appl. **18**(6), 453 (2010).
[6] C. K. Xu, H. W. Zhang, J. Parry, S. Perera, G Long, H. Zeng, Sol. Energy Mater. Sol. Cells **117**(10), 357 (2013).
[7] H. H. Sung, D. C. Tsai, Z. C. Chang, T. J. Chung, S. C. Liang, E. C. Chen, F. S. Shieu, Mater. Sci. Semicond. Process. **41**, 519 (2016).
[8] L. Q. Ouyang, D. M. Zhuang, M. Zhao, N. Zhang, X. L. Li, L Guo, R. J. Sun, M. J. Cao, Phys. Status Solidi A **212**(8), 1774 (2015).
[9] M. S. Kwon, J. Y. Kang, S.Y. Kim, J. H Kim, C. W. Jeon, Appl. Surf. Sci. **379**, 186 (2016).
[10] G M. Li, W. Liu, Y. M. Liu, S. P. Lin, X. D. Li, Y. Zhang, Z. Q. Zhou, Q. He, Y. Sun, Semicond. Sci. Technol. **30**(10), 105012 (2015).
[11] K. Kushiya, Jpn. J. Appl. Phys. **51**(10), 10NC01 (2012).
[12] C. H. Chen, W. C. Shih, C. Y. Chien, C. H. Hsu, Y. H. Wu, C. H. Lai, Sol. Energy Mater. Sol. Cells **103**(15), 25 (2012).
[13] H. Kong, J. He, X. K. Meng, L. P. Zhu, J. H. Tao, L. Sun, P.X. Yang, J.H. Chu, Mater. Lett. **118**(3), 21 (2014).
[14] J. Tian, L. Q. Peng, J. W. Chen, G Wang, X. Q. Wang, H. Kang, R. L. Wang, Appl. Phys. A **116**(4), 1813 (2014).
[15] T. R. Bai, C. Q. Liu, N. Wang, S. M. Liu, H. L. Wang, W. W. Jiang, W. Y. Ding, W. D. Fei, W. P. Chai, J. Alloys Compounds **646**, 532 (2015).
[16] L. Q. Ouyang, M. Zhao, D. M. Zhuang, J. F. Han, Z. D. Gao, L. Guo, X. L. Li, R. J. Sun, M. J. Cao, Solar Energy **118**, 375 (2015).
[17] X. L. Li, M. Zhao, D. M. Zhuang, M. J. Cao, L. Q. Ouyang, L. Guo, R. J. Sun, Z. D. Gao, Vacuum **119**, 15 (2015).
[18] H. X. Zhang, R. J. Hong, Ceramics International **42**(13), 14543 (2016).
[19] K. Cheng, Y. Q. Huang, J. J. Liu, M. Xue, Z. C. Kuang, Z. B. Lu, S. X. Wu, Z. L. Du, J. Alloys Compounds **684**, 237 (2016).
[20] T. Sakurai, N. Ishida, S. Ishizuka, M. M. Islam, A. Kasai, K. Matsubara, K. Sakurai, A. Yamada, K. Akimoto, S. Niki, Thin Solid Films **516**(20), 7036 (2008).
[21] M. H. Yeh, S. J. Ho, G H. Chen, C. W. Yeh, P. R. Chen, H. S. Chen, Solar Energy **125**, 415 (2016).
[22] M. S. Kwon, J. Y. Kang, S. Y. Kim, J. H. Kim, C. W. Jeon, Appl. Surf. Science **379**, 186 (2016).
[23] Y. M. Shin, C. S. Lee, D. H. Shin, H. S. Kwon, B. G Park, B. T. Ahn, Current Appl. Phys. **15**(1), 18 (2015).
[24] H. H. Sheu, Y. T. Hsu, S. Y. Jian, S. C. Liang, Vacuum **31**, 278 (2016).
[25] J. E. Jaffe, A. Zunger, Phys. Rev. B **64**, 241304 (2001).
[26] C. P. Muzzillo, C. E. Campbell, T. J. Anderson, J. Mater. Sci. **51**, 3362 (2016).
[27] L. Zhang, H. E. Qing, W. L. Jiang, C. J. Li, Y. Sun, Chin. Phys. Lett. **26**(2), 026801 (2006).
[28] B. Namnuan, K. Yoodee, S. Chatraphorn, J. Cryst. Growth **432**, 24 (2015).
[29] T. P. Hsieh, C. C. Chuang, C. S. Wu, J. C. Chang, J. W. Guo, W. C. Chen, Solid-State Electron. **56**(1), 175 (2011).
[30] D. Liao, A. Rockett, J. Appl. Phys. **91**(4), 1978 (2002).
[31] D. Liao, A. Rockett, Appl. Phys. Lett. **82**(17), 2829(2003).

*Corresponding author: jiulye@126.com; slban@imu.edu.cn